Measurement of the top-quark mass in the lepton+jets channel using a matrix element technique with the CDF II detector

T. Aaltonen,[21] B. Álvarez González[w],[9] S. Amerio,[41] D. Amidei,[32] A. Anastassov,[36] A. Annovi,[17] J. Antos,[12]
G. Apollinari,[15] J.A. Appel,[15] A. Apresyan,[46] T. Arisawa,[56] A. Artikov,[13] J. Asaadi,[51] W. Ashmanskas,[15]
B. Auerbach,[59] A. Aurisano,[51] F. Azfar,[40] W. Badgett,[15] A. Barbaro-Galtieri,[26] V.E. Barnes,[46] B.A. Barnett,[23]
P. Barria[dd],[44] P. Bartos,[12] M. Bauce[bb],[41] G. Bauer,[30] F. Bedeschi,[44] D. Beecher,[28] S. Behari,[23] G. Bellettini[cc],[44]
J. Bellinger,[58] D. Benjamin,[14] A. Beretvas,[15] A. Bhatti,[48] M. Binkley*,[15] D. Bisello[bb],[41] I. Bizjak[hh],[28] K.R. Bland,[5]
B. Blumenfeld,[23] A. Bocci,[14] A. Bodek,[47] D. Bortoletto,[46] J. Boudreau,[45] A. Boveia,[11] L. Brigliadori[aa],[6]
A. Brisuda,[12] C. Bromberg,[33] E. Brucken,[21] M. Bucciantonio[cc],[44] J. Budagov,[13] H.S. Budd,[47] S. Budd,[22]
K. Burkett,[15] G. Busetto[bb],[41] P. Bussey,[19] A. Buzatu,[31] C. Calancha,[29] S. Camarda,[4] M. Campanelli,[28]
M. Campbell,[32] F. Canelli[11],[15] B. Carls,[22] D. Carlsmith,[58] R. Carosi,[44] S. Carrillo[k],[16] S. Carron,[15] B. Casal,[9]
M. Casarsa,[15] A. Castro[aa],[6] P. Catastini,[20] D. Cauz,[52] V. Cavaliere,[22] M. Cavalli-Sforza,[4] A. Cerri[e],[26]
L. Cerrito[q],[28] Y.C. Chen,[1] M. Chertok,[7] G. Chiarelli,[44] G. Chlachidze,[15] F. Chlebana,[15] K. Cho,[25]
D. Chokheli,[13] J.P. Chou,[20] W.H. Chung,[58] Y.S. Chung,[47] C.I. Ciobanu,[42] M.A. Ciocci[dd],[44] A. Clark,[18]
C. Clarke,[57] G. Compostella[bb],[41] M.E. Convery,[15] J. Conway,[7] M.Corbo,[42] M. Cordelli,[17] C.A. Cox,[7] D.J. Cox,[7]
F. Crescioli[cc],[44] C. Cuenca Almenar,[59] J. Cuevas[w],[9] R. Culbertson,[15] D. Dagenhart,[15] N. d'Ascenzo[u],[42]
M. Datta,[15] P. de Barbaro,[47] S. De Cecco,[49] G. De Lorenzo,[4] M. Dell'Orso[cc],[44] C. Deluca,[4] L. Demortier,[48]
J. Deng[b],[14] M. Deninno,[6] F. Devoto,[21] M. d'Errico[bb],[41] A. Di Canto[cc],[44] B. Di Ruzza,[44] J.R. Dittmann,[5]
M. D'Onofrio,[27] S. Donati[cc],[44] P. Dong,[15] M. Dorigo,[52] T. Dorigo,[41] K. Ebina,[56] A. Elagin,[51] A. Eppig,[32]
R. Erbacher,[7] D. Errede,[22] S. Errede,[22] N. Ershaidat[z],[42] R. Eusebi,[51] H.C. Fang,[26] S. Farrington,[40] M. Feindt,[24]
J.P. Fernandez,[29] C. Ferrazza[ee],[44] R. Field,[16] G. Flanagan[s],[46] R. Forrest,[7] M.J. Frank,[5] M. Franklin,[20]
J.C. Freeman,[15] Y. Funakoshi,[56] I. Furic,[16] M. Gallinaro,[48] J. Galyardt,[10] J.E. Garcia,[18] A.F. Garfinkel,[46]
P. Garosi[dd],[44] H. Gerberich,[22] E. Gerchtein,[15] S. Giagu[ff],[49] V. Giakoumopoulou,[3] P. Giannetti,[44] K. Gibson,[45]
C.M. Ginsburg,[15] N. Giokaris,[3] P. Giromini,[17] M. Giunta,[44] G. Giurgiu,[23] V. Glagolev,[13] D. Glenzinski,[15]
M. Gold,[35] D. Goldin,[51] N. Goldschmidt,[16] A. Golossanov,[15] G. Gomez,[9] G. Gomez-Ceballos,[30] M. Goncharov,[30]
O. González,[29] I. Gorelov,[35] A.T. Goshaw,[14] K. Goulianos,[48] S. Grinstein,[4] C. Grosso-Pilcher,[11] R.C. Group[55],[15]
J. Guimaraes da Costa,[20] Z. Gunay-Unalan,[33] C. Haber,[26] S.R. Hahn,[15] E. Halkiadakis,[50] A. Hamaguchi,[39]
J.Y. Han,[47] F. Happacher,[17] K. Hara,[53] D. Hare,[50] M. Hare,[54] R.F. Harr,[57] K. Hatakeyama,[5] C. Hays,[40] M. Heck,[24]
J. Heinrich,[43] M. Herndon,[58] S. Hewamanage,[5] D. Hidas,[50] A. Hocker,[15] W. Hopkins[f],[15] D. Horn,[24] S. Hou,[1]
R.E. Hughes,[37] M. Hurwitz,[11] U. Husemann,[59] N. Hussain,[31] M. Hussein,[33] J. Huston,[33] G. Introzzi,[44] M. Iori[ff],[49]
A. Ivanov[o],[7] E. James,[15] D. Jang,[10] B. Jayatilaka,[14] E.J. Jeon,[25] M.K. Jha,[6] S. Jindariani,[15] W. Johnson,[7]
M. Jones,[46] K.K. Joo,[25] S.Y. Jun,[10] T.R. Junk,[15] T. Kamon,[51] P.E. Karchin,[57] A. Kasmi,[5] Y. Kato[n],[39]
W. Ketchum,[11] J. Keung,[43] V. Khotilovich,[51] B. Kilminster,[15] D.H. Kim,[25] H.S. Kim,[25] H.W. Kim,[25] J.E. Kim,[25]
M.J. Kim,[17] S.B. Kim,[25] S.H. Kim,[53] Y.K. Kim,[11] N. Kimura,[56] M. Kirby,[15] S. Klimenko,[16] K. Kondo*,[56]
D.J. Kong,[25] J. Konigsberg,[16] A.V. Kotwal,[14] M. Kreps,[24] J. Kroll,[43] D. Krop,[11] N. Krumnack[l],[5] M. Kruse,[14]
V. Krutelyov[c],[51] T. Kuhr,[24] M. Kurata,[53] S. Kwang,[11] A.T. Laasanen,[46] S. Lami,[44] S. Lammel,[15] M. Lancaster,[28]
R.L. Lander,[7] K. Lannon[v],[37] A. Lath,[50] G. Latino[cc],[44] T. LeCompte,[2] E. Lee,[51] H.S. Lee,[11] J.S. Lee,[25] S.W. Lee[x],[51]
S. Leo[cc],[44] S. Leone,[44] J.D. Lewis,[15] A. Limosani[r],[14] C.-J. Lin,[26] J. Linacre,[40] M. Lindgren,[15] E. Lipeles,[43]
A. Lister,[18] D.O. Litvintsev,[15] C. Liu,[45] Q. Liu,[46] T. Liu,[15] S. Lockwitz,[59] A. Loginov,[59] D. Lucchesi[bb],[41]
J. Lueck,[24] P. Lujan,[26] P. Lukens,[15] G. Lungu,[48] J. Lys,[26] R. Lysak,[12] R. Madrak,[15] K. Maeshima,[15]
K. Makhoul,[30] S. Malik,[48] G. Manca[a],[27] A. Manousakis-Katsikakis,[3] F. Margaroli,[46] C. Marino,[24] M. Martínez,[4]
R. Martínez-Ballarín,[29] P. Mastrandrea,[49] M.E. Mattson,[57] P. Mazzanti,[6] K.S. McFarland,[47] P. McIntyre,[51]
R. McNulty[i],[27] A. Mehta,[27] P. Mehtala,[21] A. Menzione,[44] C. Mesropian,[48] T. Miao,[15] D. Mietlicki,[32] A. Mitra,[1]
H. Miyake,[53] S. Moed,[20] N. Moggi,[6] M.N. Mondragon[k],[15] C.S. Moon,[25] R. Moore,[15] M.J. Morello,[15] J. Morlock,[24]
P. Movilla Fernandez,[15] A. Mukherjee,[15] Th. Muller,[24] P. Murat,[15] M. Mussini[aa],[6] J. Nachtman[m],[15] Y. Nagai,[53]
J. Naganoma,[56] I. Nakano,[38] A. Napier,[54] J. Nett,[51] C. Neu,[55] M.S. Neubauer,[22] J. Nielsen[d],[26] L. Nodulman,[2]
O. Norniella,[22] E. Nurse,[28] L. Oakes,[40] S.H. Oh,[14] Y.D. Oh,[25] I. Oksuzian,[55] T. Okusawa,[39] R. Orava,[21]
L. Ortolan,[4] S. Pagan Griso[bb],[41] C. Pagliarone,[52] E. Palencia[e],[9] V. Papadimitriou,[15] A.A. Paramonov,[2]
J. Patrick,[15] G. Pauletta[gg],[52] M. Paulini,[10] C. Paus,[30] D.E. Pellett,[7] A. Penzo,[52] T.J. Phillips,[14] G. Piacentino,[44]
E. Pianori,[43] J. Pilot,[37] K. Pitts,[22] C. Plager,[8] L. Pondrom,[58] K. Potamianos,[46] O. Poukhov*,[13] F. Prokoshin[y],[13]
A. Pronko,[15] F. Ptohos[g],[17] E. Pueschel,[10] G. Punzi[cc],[44] J. Pursley,[58] A. Rahaman,[45] V. Ramakrishnan,[58]
N. Ranjan,[46] I. Redondo,[29] P. Renton,[40] M. Rescigno,[49] T. Riddick,[28] F. Rimondi[aa],[6] L. Ristori[44],[15] A. Robson,[19]

T. Rodrigo,[9] T. Rodriguez,[43] E. Rogers,[22] S. Rolli[h],[54] R. Roser,[15] M. Rossi,[52] F. Rubbo,[15] F. Ruffini[dd],[44]
A. Ruiz,[9] J. Russ,[10] V. Rusu,[15] A. Safonov,[51] W.K. Sakumoto,[47] Y. Sakurai,[56] L. Santi[gg],[52] L. Sartori,[44]
K. Sato,[53] V. Saveliev[u],[42] A. Savoy-Navarro,[42] P. Schlabach,[15] A. Schmidt,[24] E.E. Schmidt,[15] M.P. Schmidt*,[59]
M. Schmitt,[36] T. Schwarz,[7] L. Scodellaro,[9] A. Scribano[dd],[44] F. Scuri,[44] A. Sedov,[46] S. Seidel,[35] Y. Seiya,[39]
A. Semenov,[13] F. Sforza[cc],[44] A. Sfyrla,[22] S.Z. Shalhout,[7] T. Shears,[27] P.F. Shepard,[45] M. Shimojima[t],[53]
S. Shiraishi,[11] M. Shochet,[11] I. Shreyber,[34] A. Simonenko,[13] P. Sinervo,[31] A. Sissakian*,[13] K. Sliwa,[54] J.R. Smith,[7]
F.D. Snider,[15] A. Soha,[15] S. Somalwar,[50] V. Sorin,[4] P. Squillacioti,[44] M. Stancari,[15] M. Stanitzki,[59]
R. St. Denis,[19] B. Stelzer,[31] O. Stelzer-Chilton,[31] D. Stentz,[36] J. Strologas,[35] G.L. Strycker,[32] Y. Sudo,[53]
A. Sukhanov,[16] I. Suslov,[13] K. Takemasa,[53] Y. Takeuchi,[53] J. Tang,[11] M. Tecchio,[32] P.K. Teng,[1] J. Thom[f],[15]
J. Thome,[10] G.A. Thompson,[22] E. Thomson,[43] P. Ttito-Guzmán,[29] S. Tkaczyk,[15] D. Toback,[51] S. Tokar,[12]
K. Tollefson,[33] T. Tomura,[53] D. Tonelli,[15] S. Torre,[17] D. Torretta,[15] P. Totaro,[41] M. Trovato[ee],[44] Y. Tu,[43]
F. Ukegawa,[53] S. Uozumi,[25] A. Varganov,[32] F. Vázquez[k],[16] G. Velev,[15] C. Vellidis,[3] M. Vidal,[29] I. Vila,[9]
R. Vilar,[9] J. Vizán,[9] M. Vogel,[35] G. Volpi[cc],[44] P. Wagner,[43] R.L. Wagner,[15] T. Wakisaka,[39] R. Wallny,[8]
S.M. Wang,[1] A. Warburton,[31] D. Waters,[28] M. Weinberger,[51] W.C. Wester III,[15] B. Whitehouse,[54] D. Whiteson[b],[43]
A.B. Wicklund,[2] E. Wicklund,[15] S. Wilbur,[11] F. Wick,[24] H.H. Williams,[43] J.S. Wilson,[37] P. Wilson,[15] B.L. Winer,[37]
P. Wittich[g],[15] S. Wolbers,[15] H. Wolfe,[37] T. Wright,[32] X. Wu,[18] Z. Wu,[5] K. Yamamoto,[39] J. Yamaoka,[14]
T. Yang,[15] U.K. Yang[p],[11] Y.C. Yang,[25] W.-M. Yao,[26] G.P. Yeh,[15] K. Yi[m],[15] J. Yoh,[15] K. Yorita,[56]
T. Yoshida[j],[39] G.B. Yu,[14] I. Yu,[25] S.S. Yu,[15] J.C. Yun,[15] A. Zanetti,[52] Y. Zeng,[14] and S. Zucchelli[aa6]

(CDF Collaboration[†])

[1]Institute of Physics, Academia Sinica, Taipei, Taiwan 11529, Republic of China
[2]Argonne National Laboratory, Argonne, Illinois 60439, USA
[3]University of Athens, 157 71 Athens, Greece
[4]Institut de Fisica d'Altes Energies, ICREA, Universitat Autonoma de Barcelona, E-08193, Bellaterra (Barcelona), Spain
[5]Baylor University, Waco, Texas 76798, USA
[6]Istituto Nazionale di Fisica Nucleare Bologna, [aa]University of Bologna, I-40127 Bologna, Italy
[7]University of California, Davis, Davis, California 95616, USA
[8]University of California, Los Angeles, Los Angeles, California 90024, USA
[9]Instituto de Fisica de Cantabria, CSIC-University of Cantabria, 39005 Santander, Spain
[10]Carnegie Mellon University, Pittsburgh, Pennsylvania 15213, USA
[11]Enrico Fermi Institute, University of Chicago, Chicago, Illinois 60637, USA
[12]Comenius University, 842 48 Bratislava, Slovakia; Institute of Experimental Physics, 040 01 Kosice, Slovakia
[13]Joint Institute for Nuclear Research, RU-141980 Dubna, Russia
[14]Duke University, Durham, North Carolina 27708, USA
[15]Fermi National Accelerator Laboratory, Batavia, Illinois 60510, USA
[16]University of Florida, Gainesville, Florida 32611, USA
[17]Laboratori Nazionali di Frascati, Istituto Nazionale di Fisica Nucleare, I-00044 Frascati, Italy
[18]University of Geneva, CH-1211 Geneva 4, Switzerland
[19]Glasgow University, Glasgow G12 8QQ, United Kingdom
[20]Harvard University, Cambridge, Massachusetts 02138, USA
[21]Division of High Energy Physics, Department of Physics,
University of Helsinki and Helsinki Institute of Physics, FIN-00014, Helsinki, Finland
[22]University of Illinois, Urbana, Illinois 61801, USA
[23]The Johns Hopkins University, Baltimore, Maryland 21218, USA
[24]Institut für Experimentelle Kernphysik, Karlsruhe Institute of Technology, D-76131 Karlsruhe, Germany
[25]Center for High Energy Physics: Kyungpook National University,
Daegu 702-701, Korea; Seoul National University, Seoul 151-742,
Korea; Sungkyunkwan University, Suwon 440-746,
Korea; Korea Institute of Science and Technology Information,
Daejeon 305-806, Korea; Chonnam National University, Gwangju 500-757,
Korea; Chonbuk National University, Jeonju 561-756, Korea
[26]Ernest Orlando Lawrence Berkeley National Laboratory, Berkeley, California 94720, USA
[27]University of Liverpool, Liverpool L69 7ZE, United Kingdom
[28]University College London, London WC1E 6BT, United Kingdom
[29]Centro de Investigaciones Energeticas Medioambientales y Tecnologicas, E-28040 Madrid, Spain
[30]Massachusetts Institute of Technology, Cambridge, Massachusetts 02139, USA
[31]Institute of Particle Physics: McGill University, Montréal, Québec,
Canada H3A 2T8; Simon Fraser University, Burnaby, British Columbia,
Canada V5A 1S6; University of Toronto, Toronto, Ontario,
Canada M5S 1A7; and TRIUMF, Vancouver, British Columbia, Canada V6T 2A3
[32]University of Michigan, Ann Arbor, Michigan 48109, USA

[33]*Michigan State University, East Lansing, Michigan 48824, USA*
[34]*Institution for Theoretical and Experimental Physics, ITEP, Moscow 117259, Russia*
[35]*University of New Mexico, Albuquerque, New Mexico 87131, USA*
[36]*Northwestern University, Evanston, Illinois 60208, USA*
[37]*The Ohio State University, Columbus, Ohio 43210, USA*
[38]*Okayama University, Okayama 700-8530, Japan*
[39]*Osaka City University, Osaka 588, Japan*
[40]*University of Oxford, Oxford OX1 3RH, United Kingdom*
[41]*Istituto Nazionale di Fisica Nucleare, Sezione di Padova-Trento,* [bb]*University of Padova, I-35131 Padova, Italy*
[42]*LPNHE, Universite Pierre et Marie Curie/IN2P3-CNRS, UMR7585, Paris, F-75252 France*
[43]*University of Pennsylvania, Philadelphia, Pennsylvania 19104, USA*
[44]*Istituto Nazionale di Fisica Nucleare Pisa,* [cc]*University of Pisa,*
[dd]*University of Siena and* [ee]*Scuola Normale Superiore, I-56127 Pisa, Italy*
[45]*University of Pittsburgh, Pittsburgh, Pennsylvania 15260, USA*
[46]*Purdue University, West Lafayette, Indiana 47907, USA*
[47]*University of Rochester, Rochester, New York 14627, USA*
[48]*The Rockefeller University, New York, New York 10065, USA*
[49]*Istituto Nazionale di Fisica Nucleare, Sezione di Roma 1,*
[ff]*Sapienza Università di Roma, I-00185 Roma, Italy*
[50]*Rutgers University, Piscataway, New Jersey 08855, USA*
[51]*Texas A&M University, College Station, Texas 77843, USA*
[52]*Istituto Nazionale di Fisica Nucleare Trieste/Udine,*
I-34100 Trieste, [gg]*University of Udine, I-33100 Udine, Italy*
[53]*University of Tsukuba, Tsukuba, Ibaraki 305, Japan*
[54]*Tufts University, Medford, Massachusetts 02155, USA*
[55]*University of Virginia, Charlottesville, Virginia 22906, USA*
[56]*Waseda University, Tokyo 169, Japan*
[57]*Wayne State University, Detroit, Michigan 48201, USA*
[58]*University of Wisconsin, Madison, Wisconsin 53706, USA*
[59]*Yale University, New Haven, Connecticut 06520, USA*
(Dated: August 8, 2011)

A measurement of the top-quark mass is presented using Tevatron data from proton-antiproton collisions at center-of-mass energy $\sqrt{s} = 1.96$ TeV collected with the CDF II detector. Events are selected from a sample of candidates for production of $t\bar{t}$ pairs that decay into the lepton+jets channel. The top-quark mass is measured with an unbinned maximum likelihood method where the event probability density functions are calculated using signal and background matrix elements, as well as a set of parameterized jet-to-parton transfer functions. The likelihood function is maximized with respect to the top-quark mass, the signal fraction in the sample, and a correction to the jet energy scale (JES) calibration of the calorimeter jets. The simultaneous measurement of the JES correction (Δ_{JES}) amounts to an additional *in situ* jet energy calibration based on the known mass of the hadronically decaying W boson. Using the data sample of 578 lepton+jets candidate events, corresponding to 3.2 fb^{-1} of integrated luminosity, the top-quark mass is measured to be $m_t = 172.4 \pm 1.4 \,(\mathrm{stat} + \Delta_{\mathrm{JES}}) \pm 1.3 \,(\mathrm{syst})$ GeV/c^2.

———

———

[*]Deceased

[†]With visitors from [a]Istituto Nazionale di Fisica Nucleare, Sezione di Cagliari, 09042 Monserrato (Cagliari), Italy, [b]University of CA Irvine, Irvine, CA 92697, USA, [c]University of CA Santa Barbara, Santa Barbara, CA 93106, USA, [d]University of CA Santa Cruz, Santa Cruz, CA 95064, USA, [e]CERN,CH-1211 Geneva, Switzerland, [f]Cornell University, Ithaca, NY 14853, USA, [g]University of Cyprus, Nicosia CY-1678, Cyprus, [h]Office of Science, U.S. Department of Energy, Washington, DC 20585, USA, [i]University College Dublin, Dublin 4, Ireland, [j]University of Fukui, Fukui City, Fukui Prefecture, Japan 910-0017, [k]Universidad Iberoamericana, Mexico D.F., Mexico, [l]Iowa State University, Ames, IA 50011, USA, [m]University of Iowa, Iowa City, IA 52242, USA, [n]Kinki University, Higashi-Osaka City, Japan 577-8502, [o]Kansas State University, Manhattan, KS 66506, USA, [p]University of Manchester, Manchester M13 9PL, United Kingdom, [q]Queen Mary, University of London, London, E1 4NS, United Kingdom, [r]University of Melbourne, Victoria 3010, Australia, [s]Muons, Inc., Batavia, IL 60510, USA, [t]Nagasaki Institute of Applied Science, Nagasaki, Japan, [u]National Research Nuclear University, Moscow, Russia, [v]University of Notre Dame, Notre Dame, IN 46556, USA, [w]Universidad de Oviedo, E-33007 Oviedo, Spain, [x]Texas Tech University, Lubbock, TX 79609, USA, [y]Universidad Tecnica Federico Santa Maria, 110v Valparaiso, Chile, [z]Yarmouk University, Irbid 211-63, Jordan, [hh]On leave from J. Stefan Institute, Ljubljana, Slovenia,

The top-quark mass, m_t, is an intrinsic parameter of the standard model (SM) of particle physics and is of particular importance due to its strikingly large value. As a result, the top quark has a large effect on radiative corrections to electroweak processes and has a Yukawa coupling to the Higgs field of $\mathcal{O}(1)$, which may provide insight into the mechanism of electroweak symmetry breaking [1].

The Higgs boson mass, m_H, is not predicted by the SM, but constraints on its value can be derived from the calculation of radiative corrections to the W boson mass, m_W, and from the values of the other precision electroweak variables [2]. These corrections depend primarily on $\ln m_H$ and m_t^2, and thus precision measurements of m_W and m_t provide important constraints on m_H.

The dominant top-quark production process is pair production via the strong interaction. At Fermilab's Tevatron this process is initiated by $p\bar{p}$ collisions at center-of-mass energy $\sqrt{s} = 1.96$ TeV. Because of its large mass, the top quark decays rapidly with lifetime $\tau_t \sim 10^{-25}$ s [3] — fast enough that it has essentially no time to interact and may be considered as a free quark. This allows a direct measurement of its mass from the daughter particles from its decay, and as a result m_t has the lowest relative uncertainty of all of the quark masses [4].

In the SM top quarks decay via the weak interaction, predominantly to W bosons and b quarks as $t\bar{t} \rightarrow W^+bW^-\bar{b}$. W bosons decay into lower-mass fermion-antifermion pairs: a charged lepton and a neutrino ($W^+ \rightarrow \bar{\ell}\nu_\ell$ and $W^- \rightarrow \ell\bar{\nu}_\ell$), "leptonic decay"; or an up-type quark and a down-type quark ($W^+ \rightarrow q\bar{q}'$ and $W^- \rightarrow \bar{q}q'$), "hadronic decay". The result presented here uses the lepton+jets decay channel (with $q\bar{q}'b\ell\bar{\nu}_\ell\bar{b}$ or $\bar{\ell}\nu_\ell b\bar{q}q'\bar{b}$ in the final state), where one of the two W bosons decays leptonically into an electron or a muon, and the other decays hadronically. All the quarks in the final state evolve into jets of hadrons. Events with tau leptons were not selected directly, but may contribute a few percent of the total sample via leptonic cascade decays or fake jets. The most recent m_t measurements obtained at the Tevatron using the lepton+jets topology are reported in Ref. [5], while the results of an earlier version of the present analysis using 955 pb^{-1} of integrated luminosity are reported in Ref. [6]. The distinctive feature of this analysis is the use of matrix element calculations to describe the dominant background contribution. The result presented here uses a more than three times larger data sample than the earlier version, and employs a more detailed likelihood function.

The leptons and jets resulting from the top-antitop quark pair ($t\bar{t}$) decay are detected in the CDF II general-purpose particle detector that is described in detail elsewhere [7]. Azimuthally and forward-backward symmetric about the beam-line, the detector contains a high precision particle tracking system immersed in a 1.4 T magnetic field and surrounded by calorimetry, with muon detectors on the outside. A right-handed spherical co-

Electron	E_T > 20 GeV	$|\eta|$ < 1.1
or Muon	p_T > 20 GeV/c	$|\eta|$ < 1.0
$\not{E}_T$	$\not{E}_T$ > 20 GeV	$|\eta|$ < 3.6
Jets	E_T > 20 GeV	$|\eta|$ < 2.0
Four jets; at least one from a b quark		

TABLE I: Event selection criteria.

ordinate system is employed, with the polar angle θ measured from the proton beam direction, the azimuthal angle ϕ in the plane perpendicular to the beam-line, and the distance r from the center of the detector. Transverse energy and momentum are defined as $E_T \equiv E\sin\theta$ and $p_T \equiv p\sin\theta$, where E and p denote energy and momentum. Pseudorapidity is defined as $\eta \equiv -\ln\tan(\theta/2)$.

This measurement makes use of CDF II data collected between February 2002 and August 2008, representing approximately 3.2 fb^{-1} of integrated luminosity. The event selection criteria (Table I) are tuned to select the lepton+jets final-state particles, requiring that each event must have exactly one high-E_T electron or high-p_T muon, exactly four high-E_T jets, and a significant amount of missing E_T, $\not{E}_T$ [8], characteristic of the undetected neutrino. Jets are reconstructed using a cone algorithm [9], with the cone radius $\Delta R \equiv \sqrt{(\Delta\eta)^2 + (\Delta\phi)^2} = 0.4$. At least one of the four jets must be identified as originating from a b quark via the SECVTX algorithm [10], which detects displaced secondary vertices characteristic of the decay of long-lived b hadrons. A total of 578 events are selected, of which 76% are expected to be $t\bar{t}$ events (Table II). Of the 24% of events expected to be background, it is predicted that 69% arise from the production of a W boson in conjunction with 4 jets (W+jets), 19% come from multi-jet QCD production (non-W), while the remaining 12% are from sources such as diboson and single-top-quark production. These fractions are estimated using theoretical cross-sections, Monte Carlo (MC) simulated events, and data. The $t\bar{t}$ events are generated using the Lund Monte Carlo program PYTHIA [11], with a top-quark mass of 175 GeV/c^2 and a $t\bar{t}$ production cross section of 6.7 ± 0.8 pb [12]. The W+jets and Z+jets events are generated using the ALPGEN generator [13] while the single-top-quark events are generated using the MADEVENT package [14], in both cases also using PYTHIA to perform the parton showering and hadronization. Diboson events are also generated using PYTHIA. In addition, data are used for non-W events [15].

This analysis employs an unbinned maximum likelihood method [6, 16, 17]. The m_t-dependent probability density function (p.d.f.) is calculated for each event in the data sample:

$$\mathcal{P}(k) = \nu_{\text{sig}}P_s(k) + (1 - \nu_{\text{sig}})P_b(k), \qquad (1)$$

where $k \equiv (E_i, \vec{p}_i)$ represents the measured kinematic

sample	# of events	% of total	% of bkg
$t\bar{t}$ signal	425.0 ± 58.9	76.0%	-
W+jets	92.6 ± 15.9	16.6%	69.0%
non-W	25.0 ± 12.5	4.5%	18.7%
single top quark	6.6 ± 0.4	1.2%	4.9%
diboson	6.0 ± 0.6	1.1%	4.5%
Z+jets	3.9 ± 0.5	0.7%	2.9%
total	559.2 ± 67.0	100%	-
Observed	578		

TABLE II: Number of expected signal and background events, corresponding to the total integrated luminosity of 3.2 fb^{-1} . The percentages are used when generating Monte Carlo simulated experiments.

quantities of the event, P_s and P_b are respectively the normalized p.d.f.s for signal and background events, and $\nu_{\rm sig}$ is the signal fraction parameter (constrained $0 \leq \nu_{\rm sig} \leq 1$). Signal events are defined as events consistent with $q\bar{q} \rightarrow t\bar{t}$ production and $t\bar{t}$ decay into the lepton+jets channel, as described by the leading-order (LO) matrix element evaluated by Mahlon and Parke [18]. Background events are assumed to be described by a matrix element for W+jets production, which is calculated using a sum of 1286 W+4-partons amplitudes for 592 subprocesses encoded in the VECBOS MC event generator [19]. This approximation does mean that there are some events that, in principle, are not described by either P_s or P_b, including non-W, single top, diboson, Z+jets, and $W + b\bar{b}$+2-partons events, as well as W+jets events from W+0-, 1-, 2- and 3-partons processes. However, studies with MC simulated events show that the ratio P_b/P_s calculated for all of these event types is similar to that for W+4-partons events, and that, in practice, such events mostly contribute to the likelihood function via the P_b term and do not add any more bias than the W+4-partons events or than the poorly reconstructed $t\bar{t}$ events themselves [20]. Any residual bias in the measured top-quark mass is removed at the end, as described later in the paper.

The signal and background p.d.f.s, P_s and P_b, are constructed in analogous fashions, starting with the appropriately normalized parton-level differential cross-section [4], $d\hat{\sigma}_s$ or $d\hat{\sigma}_b$, which is then convolved with parton distribution functions (PDFs) and a jet-to-parton transfer function $W(k, \varkappa)$. P_s is thus given by

$$P_s(k; m_t, \Delta_{\rm JES}) = \frac{1}{n_{jp}} \sum_{\rm jet\ perm.}^{n_{jp}} \frac{1}{\hat{\sigma}_s(m_t)} \frac{1}{A_s(m_t, \Delta_{\rm JES})} \times$$
(2)
$$\int d\hat{\sigma}_s(\varkappa; m_t)\, dx_{\rm Bj}^1 dx_{\rm Bj}^2\, W(k, \varkappa; \Delta_{\rm JES})\, f(x_{\rm Bj}^1)(x_{\rm Bj}^2),$$

where $\varkappa \equiv (\varepsilon_i, \vec{\pi}_i)$ represents the actual event parton-level kinematic quantities corresponding to the measured quantities k, and parameter $\Delta_{\rm JES}$ is defined in the next

paragraph. The PDFs $f(x_{\rm Bj})$ define the probability density for a colliding parton to carry a longitudinal momentum fraction $x_{\rm Bj}$ and are given by CTEQ5L [21]. A_s is the mean acceptance function for signal events, a normalization term that is the consequence of the constriction of the phase-space of the integral by the event selection cuts and by the detector acceptance. The average over the jet permutations, n_{jp}, is due to ambiguity in assigning final state jets to partons. The fact that the two light quarks in the final state are indistinguishable allows the reduction from the original 24 permutations to 12 in the expression for P_s, and the b-tagging information allows a further reduction to 6 assignments for events with one identified b-jet and 2 for events with both b-jets identified. In the similar expression for P_b, all 24 permutations are averaged.

The jet-to-parton transfer function $W(k, \varkappa)$ is a p.d.f. describing the probability density for an event with outgoing partons and charged lepton with $\varkappa$ to be measured as reconstructed k. The charged lepton is assumed to be well-measured, allowing the use of a Dirac δ-function to represent the mapping between its parton-level momentum, $\vec{\pi}_\ell$, and its reconstructed momentum, $\vec{p}_\ell$. For the four jets, the function is obtained by parameterizing the jet-to-parton mapping observed in fully simulated PYTHIA $t\bar{t}$ events. These events contain all of the information about the original partons as well as the measured jets. The simulation includes physical effects, such as radiation and hadronization, as well as the effects of measurement resolution and of the jet reconstruction algorithm. The parameterization is made in two parts that are assumed to be independent: the energy transfer function W_E, describing the jet energies E, and the angular transfer function W_A, describing the mapping for the jet angles. The jet-to-parton transfer function is thus given by

$$W(k, \varkappa; \Delta_{\rm JES}) = \delta^3(\vec{p}_\ell - \vec{\pi}_\ell)\, W_A$$
(3)
$$\times \prod_{i=1}^{4} \left(\frac{1}{E_i p_i} W_E^i(E_i, \varepsilon_i; \Delta_{\rm JES}) \right).$$

The reconstructed jet energies, E_i, used in the function W_E are not just the raw calorimeter energy deposits, but are first calibrated so that they represent the combined energies released in the calorimeter by the many particles constituting each jet. This is achieved using the CDF jet energy scale (JES) calibration [22], which is subject to a significant systematic uncertainty. The uncertainties of individual jet energy measurements, $\sigma(E_i)$, are therefore correlated, and their fractional JES uncertainty, $\sigma(E_i)/E_i$, is typically $\sim 3\%$. If this were included as a systematic uncertainty on the measured m_t it would reduce the measurement precision drastically; in fact, each 1% of fractional JES uncertainty would add about 1 GeV/c^2 uncertainty to the measured m_t [23] . However, such a treatment overestimates the uncertainty because the energies of the two daughter jets of the
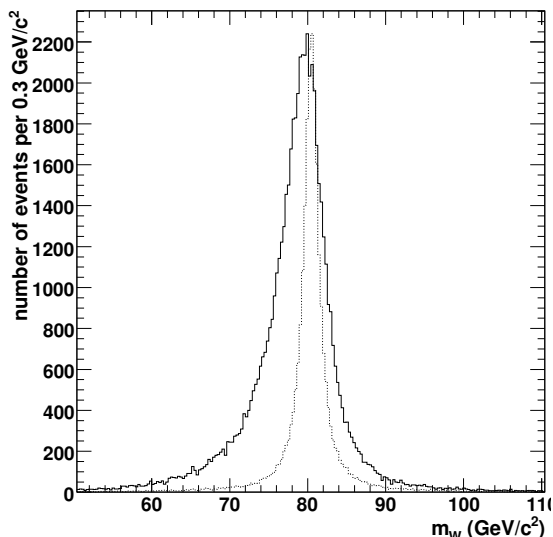
FIG. 1: The reconstructed 2-jet invariant mass of the hadronically decaying W boson, m_W, for measured jet angles (solid line) and for parton-level angles (dotted line), obtained after assuming the primary parton energy as jet energy. For ease of comparison, the parton-level distribution is renormalized, so that the maxima of the two distributions are the same.

hadronically decaying W boson can be constrained based on the known W boson mass. Applying this constraint to all events in the data sample while allowing the jet energies to be shifted results in the *in situ* measurement of the JES correction, $\Delta_{\rm JES}$, defined as the number of $\sigma(E_i)$ values by which the energy of each jet is shifted in the likelihood fit. This effectively re-calibrates the measured jet energies based on the known W boson mass and replaces a large component of the JES systematic uncertainty with a much smaller statistical uncertainty on the $\Delta_{\rm JES}$. The $\Delta_{\rm JES}$ dependence of the jet energies is included in the parameterization of the function W_E. This parameterization is made in eight bins in pseudorapidity $|\eta|$, separately for light and b-jets, using a sum of two Gaussians as a function of the difference between the parton energies and the corrected jet energies as measured in a sample of MC simulated events which pass the same selection criteria as the data.

In an earlier version of this analysis [6], the jet-to-parton transfer functions for all jet angles were approximated by Dirac δ-functions. The introduction of the function W_A was motivated by a discrepancy noticed in simulated $t\bar{t}$ events in the 2-jet effective invariant mass of the hadronically decaying W boson, m_W. Even when the true simulated parton-level jet energies are used, instead of the corresponding reconstructed detector-level values, the use of the measured jet angles rather than their parton-level values causes a significant shift of the reconstructed m_W from its nominal value, as illustrated in Fig. 1.

There is also a negative skewness in the distribution

for measured angles, and since parton-level jet energies are used, the observed effects are due to the differences between the measured angles and the parton-level angles alone. The peak of the m_W distribution, when fit by a Breit-Wigner distribution, corresponds to a W boson pole mass of 79.5 GeV/c^2, a -0.9 GeV/c^2 shift from its parton-level value of 80.4 GeV/c^2. This is found to be a result of a correlation between the measured jet directions: the measured angle, α_{12}, between the two jets is, on average, reduced so that the two jets appear closer together than their parent partons, e.g. see Fig. 2. Since the apparent W boson mass is utilized to measure $\Delta_{\rm JES}$ and thus calibrate the measured jet energies, a jet-to-parton transfer function describing the change in the angle α_{12} is important in making an accurate measurement of $\Delta_{\rm JES}$ and thus the top-quark mass. The function W_A also describes a much smaller correlation effect seen in the angle α_{Wb} between the hadronic-side b-jet and the hadronically decaying W boson. The function W_A is thus parameterized using two different functions, W_A^{12} and W_A^{Wb}, describing the mappings for the angles α_{12} and α_{Wb}. The remaining angles describe resolution effects rather than the correlations and, due to computational constraints, are assumed to be well measured with their contributions to W_A approximated by Dirac delta functions.

The functions W_A^{12} and W_A^{Wb} are both fit using a sum of a skew-Cauchy distribution and two Gaussians, describing the change in the cosine of the relevant angle, $\Delta \cos(\alpha_{12})$ and $\Delta \cos(\alpha_{Wb})$, from partons to measured jets. Since the correlation effects are stronger in jets that are closer together, the functions are parameterized in bins of $\cos(\alpha_{12})$ and $\cos(\alpha_{Wb})$, respectively; one example for each function is shown in Fig. 2.

The m_W distribution after convolution with the function W_A is shown in Fig. 3. The skewness is removed and the mean value agrees well with the parton-level distribution.

The 20 integration variables (3 for each final-state particle and the $x_{\rm Bj}$ for each initial state parton, assuming zero transverse momentum for the $t\bar{t}$ pair) in the expression for the signal and background p.d.f.s (Eq. 2) are reduced to 16 by integrating over the 4-momentum conservation Dirac δ-function inherent in the expression for $d\hat{\sigma}_s$. The charged lepton 3-momentum integration and all but two of the jet angular integrations are made trivial by the Dirac δ-functions in the function $W(k, \varkappa)$, leaving 7 integration variables. In P_s, this is further reduced to 5 variables via a change of variables to the squared masses of the top quarks and by using the narrow-width approximation for the Breit-Wigner distributions of both top-quark decays in the $t\bar{t}$ matrix element. The integral is then evaluated using the VEGAS [24] adaptive Monte Carlo integration algorithm [6], which uses importance sampling, which means that the sample points are concentrated in the regions that make the largest contribution to the integral.

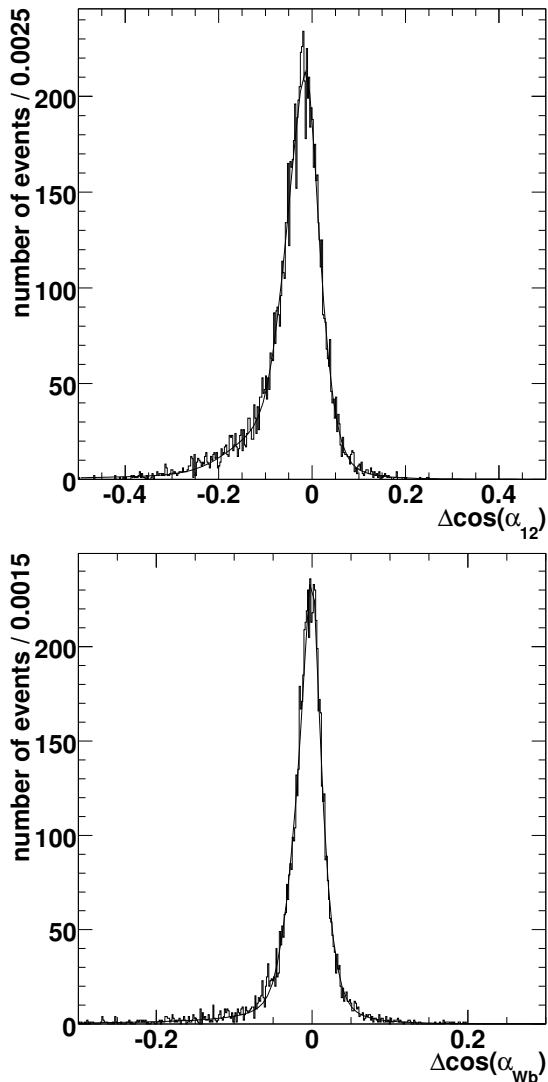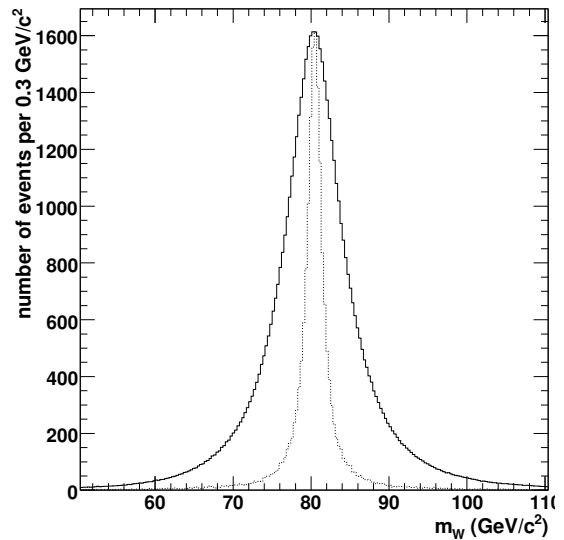The treatment of P_b is unchanged since the previous

FIG. 3: The m_W distribution for measured angles from Fig. 1 is plotted (solid line) after convolution with the function W_A. For ease of comparison, the parton-level distribution (dotted line) is normalized so that the maxima of the two distributions are the same.

FIG. 2: Examples of parameterization of the functions W_A^{12} and W_A^{Wb} in the bins where $0.2 < \cos{(\alpha_{12})} < 0.4$ and $0.2 < \cos{(\alpha_{Wb})} < 0.4$. The histograms show MC simulation events and the curves represent the parameterization.

version of this analysis [6], except for the updated energy transfer function W_E. The integrand in the expression for P_b is much more computationally intensive than for P_s and a simplified Monte Carlo method of integration is employed, giving reasonable convergence with an execution time comparable to that of P_s. The simplifications used in this computation of P_b include setting the function W_A to a Dirac δ-function for all angles, using a narrow width approximation for the W boson decay, and neglecting the Δ_{JES} dependence of the function W_E. Therefore, the value of P_b for each event does not depend on the likelihood parameters m_t and Δ_{JES}, while P_s is a two-dimensional function of those parameters [6]. In this approximation, the product of the background p.d.f. normalization terms (corresponding to the variables $\hat{\sigma}_b \cdot A_b$

in Eq. 2) is set to a constant, whose value is chosen to optimize the statistical sensitivity of the method, effectively providing an appropriate relative normalization with respect to P_s.

The log-likelihood function is given as a sum over the 578 events in the sample:

$$\ln \mathcal{L}(k; m_t, \Delta_{\text{JES}}, \nu_{\text{sig}}) = \qquad (4)$$

$$\sum_{i=1}^{578} \ln \left[\nu_{\text{sig}} P_s(k_i; m_t, \Delta_{\text{JES}}) + (1 - \nu_{\text{sig}}) P_b(k_i) \right].$$

It is calculated on a two-dimensional 31×17 grid in m_t and Δ_{JES}, spanning $145 \le \text{m}_t \le 205$ GeV/c^2 and $-4.8 \le \Delta_{\text{JES}} \le 4.8$, with a spacing between grid points of 2 GeV/c^2 in m_t and 0.6 in Δ_{JES}. To optimize computational time, the bin size is chosen to be as large as possible without appreciably affecting the fit result. The third likelihood parameter, the signal fraction parameter ν_{sig}, is allowed to vary continuously (within the constraint $0 \le \nu_{\text{sig}} \le 1$), and the likelihood function is maximized with respect to ν_{sig} at each point on the grid using the MINUIT program [25]. The resulting surface described on the grid is the maximized profile log-likelihood at ν_{sig}. The top-quark mass, m_t, and the jet energy scale correction, Δ_{JES}, are measured by making a two-dimensional parabolic fit to the surface, consistent with the expectation for the likelihood function to be Gaussian near its maximum. The maximum of the parabola gives the measured m_t and Δ_{JES}, while the measured ν_{sig} is taken from its value at the grid point of maximum likelihood. The estimated one-σ statistical uncertainty of the mea-

surement is represented by the ellipse corresponding to a change in log-likelihood $\Delta \ln \mathcal{L} = 0.5$ from the maximum of the fitted parabola. The values of m_t and $\Delta_{\rm JES}$ are found to be anti-correlated (Fig. 4). No correlation is observed between $\nu_{\rm sig}$ and m_t or $\Delta_{\rm JES}$.

The accuracy of the measured m_t and $\Delta_{\rm JES}$, and their uncertainties, are checked using ensembles of MC simulated experiments, using the MC samples previously mentioned with the addition of 22 $t\bar{t}$ samples generated with values of m_t between 161 and 185 GeV/c^2. The numbers of $t\bar{t}$ events and those of the various backgrounds are Poisson fluctuated around the values shown in Table II. Studies of the relationships between the known input simulation parameters and their corresponding measurements show no evidence of bias when a clean sample of MC simulated $t\bar{t}$ events is used. The clean sample contains only $t\bar{t}$ events in the l+jets channel and with only the correct jet-parton matching. However, the presence of signal events with jets which are poorly or incorrectly matched to partons and events which do not match the decay hypothesis biases the likelihood fit result and increases the pull width. The presence of background events also biases the fit, due to the backgrounds that are not well described by P_b and the approximations in P_b. The bias is removed using a set of functions obtained from a fit to the MC simulation and parameterized in terms of the measured m_t, $\Delta_{\rm JES}$ and $\nu_{\rm sig}$ [20]. This amounts to adding 1.1 GeV/c^2 to the m_t value produced by the likelihood fit and multiplying the uncertainties by 1.26 so that the pull widths are consistent with unity. The systematic uncertainty due to this measurement calibration is small, as shown in Table III.

Despite the reduction from the *in situ* $\Delta_{\rm JES}$ calibration, the remaining JES component of the systematic uncertainty on m_t is still one of the largest systematic uncertainties of the measurement (Table III). Other significant systematic uncertainties are mainly a result of assumptions made in the simulation of the events that are used in the tuning and calibration of the measurement method. In most cases, they are evaluated by varying different aspects of the MC simulation, e.g. signal MC generator (PYTHIA versus HERWIG [26]), color reconnection model tune (Apro versus ACRpro [27–29]), and parameters of initial and final state radiation (ISR and FSR). A detailed description of the remaining systematic effects has been published elsewhere [30]. The systematic uncertainties for each effect are added in quadrature, resulting in a total estimated systematic uncertainty of 1.3 GeV/c^2 (Table III).

The measurement is made using the data sample of 578 events, yielding

$$m_t = 172.4 \pm 1.4 \, (\text{stat}+\Delta_{\rm JES}) \pm 1.3 \, (\text{sys}) \ {\rm GeV}/c^2$$
$$m_t = 172.4 \pm 1.9 \, (\text{total}) \ {\rm GeV}/c^2, \tag{5}$$

with $\Delta_{\rm JES} = 0.3 \pm 0.3$ (stat). The central value and the contour ellipses corresponding to the one-, two- and three-σ statistical confidence intervals (68.3%, 95.4%,

Systematic	(GeV/c^2)
MC Generator	0.70
Residual JES	0.65
Color Reconnection	0.56
b-jet energy	0.39
Background	0.45
ISR and FSR	0.23
Multiple Hadron Interactions	0.22
PDFs	0.13
Lepton Energy	0.12
Measurement Calibration	0.12
Total	1.31

TABLE III: Contributions to the total expected systematic uncertainty.
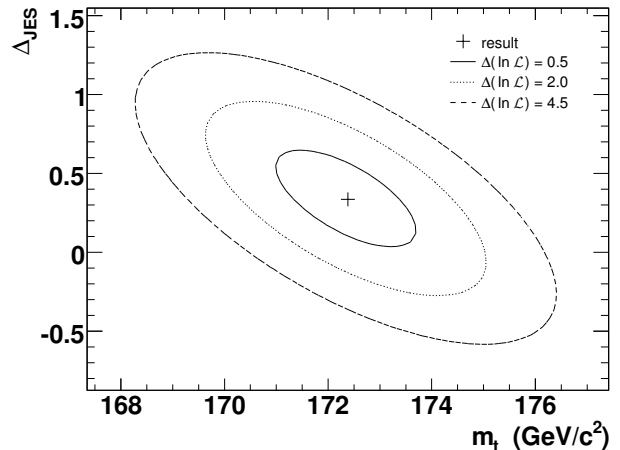

FIG. 4: The measurement result and the contour ellipses of the parabolic fit corresponding to the one-, two- and three-σ confidence intervals for the statistical uncertainty on m_t and $\Delta_{\rm JES}$.

and 99.7% confidence levels) of the measurement are illustrated in Fig. 4. The overall statistical uncertainty on the measured top-quark mass is labeled "stat+$\Delta_{\rm JES}$" because it includes the uncertainty on m_t due to the statistical uncertainty on the measured $\Delta_{\rm JES}$, i.e. the uncertainty is given by half of the full width of the one-σ contour of Fig. 4.

In conclusion, a precise measurement of the top-quark mass has been presented using CDF lepton+jets candidate events corresponding to an integrated luminosity of 3.2 fb^{-1} . Using an improved matrix element method with an *in situ* jet energy calibration we measure $m_t = 172.4 \pm 1.9$ GeV/c^2.

[1] G. Bhattacharyya, Rept. Prog. Phys. **74**, 026201 (2011), for example, and references therein.

[2] LEP and Tevatron Electroweak Working Groups, and SLD electroweak heavy flavour groups (ALEPH, CDF, D0, DELPHI, L3, OPAL and SLD Collaborations) (2010), `arXiv:1012.2367`.

[3] V. M. Abazov et al. (D0 Collaboration), Phys. Rev. Lett. **106**, 022001 (2011).

[4] K. Nakamura et al. (Particle Data Group), J. Phys. **G37**, 075021 (2010).

[5] Tevatron Electroweak Working Group (CDF and D0 Collaborations) (2010), `arXiv:1007.3178`.

[6] A. Abulencia et al. (CDF Collaboration), Phys. Rev. Lett. **99**, 182002 (2007).

[7] R. Blair et al. (CDF Collaboration) (1996), `FERMILAB-PUB-96-390-E`.

[8] A. Abulencia et al. (CDF Collaboration), Phys. Rev. **D74**, 072006 (2006), we define $\not{E}_T = \left| -\sum_i E_T^i \hat{n}_i \right|$, where $i =$ calorimeter tower number with $|\eta| < 3.6$ and $\hat{n}_i$ is a unit vector perpendicular to the beam axis and pointing at the ith calorimeter tower.

[9] F. Abe et al. (CDF Collaboration), Phys. Rev. **D45**, 1448 (1992).

[10] D. E. Acosta et al. (CDF Collaboration), Phys. Rev. **D71**, 052003 (2005).

[11] T. Sjostrand, S. Mrenna, and P. Skands, JHEP **05**, 026 (2006).

[12] N. Kidonakis and R. Vogt, Phys. Rev. D **68**, 114014 (2003).

[13] M. L. Mangano, M. Moretti, F. Piccinini, R. Pittau, and A. D. Polosa, JHEP **07**, 001 (2003).

[14] J. Alwall et al., JHEP **09**, 028 (2007).

[15] D. E. Acosta et al. (CDF Collaboration), Phys. Rev. **D71**, 072005 (2005).

[16] V. M. Abazov et al. (D0 Collaboration), Nature **429**, 638 (2004).

[17] V. M. Abazov et al. (D0 Collaboration), Phys. Lett. **B617**, 1 (2005).

[18] G. Mahlon and S. J. Parke, Phys. Rev. **D53**, 4886 (1996).

[19] F. A. Berends, H. Kuijf, B. Tausk, and W. T. Giele, Nuclear Physics B **357**, 32 (1991).

[20] J. T. Linacre (2010), `FERMILAB-THESIS-2010-05`.

[21] H. L. Lai et al. (CTEQ Collaboration), Eur. Phys. J. **C12**, 375 (2000).

[22] A. Bhatti et al., Nucl. Instrum. Meth. **A566**, 375 (2006).

[23] T. Affolder et al., Physical Review D **63**, 032003 (2001).

[24] G. P. Lepage, J. Comput. Phys. **27**, 192 (1978).

[25] F. James, *Minuit - function minimization and error analysis - reference manual* (2000), URL `http://wwwasdoc.web.cern.ch/wwwasdoc/minuit/minmain.html`.

[26] G. Corcella et al. (2002), `arXiv:hep-ph/0210213`.

[27] P. Z. Skands and D. Wicke, Eur. Phys. J. **C52**, 133 (2007).

[28] D. Wicke and P. Z. Skands, Nuovo Cim. **123B**, S1 (2008).

[29] P. Z. Skands (2009), `FERMILAB-CONF-09-113-T`, arXiv:0905.3418.

[30] T. Aaltonen et al. (CDF Collaboration), Phys. Rev. **D79**, 072001 (2009).